Two Gratings Talbot Bands Spectral Domain Interferometer

MANUEL J. MARQUES[1,*], ADRIAN BRADU[1], AND ADRIAN PODOLEANU[1]

[1]Applied Optics Group, School of Physical Sciences, University of Kent, Canterbury CT2 7NH, United Kingdom
[*]Corresponding author: mjmm2@kent.ac.uk

Compiled July 29, 2015

A configuration for Talbot bands is presented, where two tilted gratings replace the splitter normally used for recombining the signals from the two interferometer arms. The two optical beams from the interferometer are launched by two fiber leads tightly brought together in the front focal plane of a collimating lens. As the tips of the two fibers are slightly off-axis, the emergent beams after the collimating lens are not parallel. In combination with the two tilted gratings, the non parallel launching of the two beams leads to total elimination of mirror terms even when the two beams overlap on either grating. The effects of several geometrical parameters on the visibility performance versus optical path difference between the two arm lengths of the interferometer are evaluated.

OCIS codes: *(120.6200) Spectrometers and spectroscopic instrumentation; (120.3180) Inteferometry; (050.0050) Diffraction and gratings; (060.1810) Buffers, couplers, routers, switches, and multiplexers; (120.0120) Instrumentation, measurement, and metrology*

http://dx.doi.org/10.1364/ao.XX.XXXXXX

Talbot bands (TB) [1–4] represent a particular case of modulation of the channeled spectrum at the output of an interferometer illuminated by a broadband optical source. This modulation takes place for only one sign of the optical path difference (OPD) in the interferometer. In other words, a TB configuration can determine which optical path of the two interfering beams is longer or shorter than the other one. In optical coherence tomography (OCT) applications, the inability to make distinction between the two signs of the OPD leads to superposition of cross section images due to the positive and the negative OPD. This is known as the problem of mirror terms [2, 5]. Several mirror term removal methods have been described in the literature, such as sequential phase-shifting interferometry [6], phase shifting using a 3x3 splitter [7], resorting to phase modulation [8] or dispersion [9] to restore the full range and address the ambiguity of the OPD sign. These methods, however, require several images or steps in order to attenuate the mirror terms [12]. A TB configuration only requires a single spectral acquisition and no post-processing.

Previous studies of Talbot bands [2] have shown that the difference between conventional spectral interferometry configurations and Talbot bands configurations lies in the order that the two operations, interference and diffraction, are performed. In conventional spectral interferometry, the beams from the object and reference arms are first superposed, with the result being then sent to a spectrometer, i.e. interference is followed by diffraction on a grating or dispersion in a prism [10]. In these configurations, positive and negative OPD values of the same OPD modulus produce the same channeled spectrum modulation, i.e. such configuration cannot distinguish between positive and negative OPD values, as shown by the symmetric curve C_1 in Fig. 1. In a TB configuration, the two beams interfere on the line camera used in the spectrometer after the diffraction operation has been carried out. In all previous reports on TB configurations, the two beams from the interferometer are collimated and are sent parallel to each other to a single diffraction grating. Let us consider a gap, g, between the centers of the two beams, each of them determining a footprint with a beam diameter S on the grating. A TB configuration can be switched to a non-TB configuration by controlling the gap g. As long as g is at least equal to S, TB behavior is obtained, as depicted by the curve C_3 in Fig. 1. If however the beams are separated by less than S, the overlapping parts of the two beams exhibit interference first and diffraction after. These overlapping parts

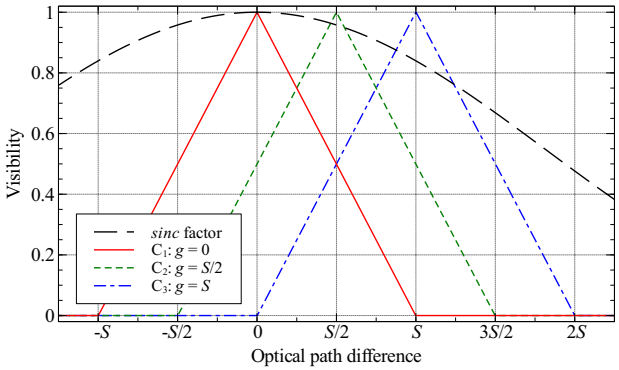

Fig. 1. *(color online)* Qualitative illustration of SDI intensity versus OPD in a set-up consisting of an interferometer and a single grating. The curves $C_2 - C_3$ represent the correlation of power distribution within the two footprints of the incident beams on a single grating for different values of the spatial gap g between the beam centers [11]. The footprints are considered for simplicity as top hats with widths $S = 4$ mm. The wider profile above (black dashed) is determined by the *sinc* factor [13]. The shifting along the OPD axis in curves $C_2 - C_3$ is determined by the gap, g, between the two interfering beams.

determine modulation of the channeled spectrum that is independent on the OPD sign, i.e. mirror terms are reinstated, as shown by the curve C_2 in Fig. 1 for $g = S/2$. All the curves represented in Fig. 1 are simulation results from a spectrometer with a single diffraction grating where the beams projected onto it have a varying gap g between them.

Previous reports on Talbot bands [2, 12] developed the explanation of the visibility curve versus OPD as determined by the product of C (shown in Fig. 1 for three values of gap g) with a *sinc* factor. The factor C, as detailed in [11] and further documented below, incorporates the properties of Talbot bands whilst the *sinc* factor includes the spectrometer resolution determined by the optical bandwidth of light on each pixels of the line camera in the spectrometer [13].

A Mach-Zehnder configuration may be employed for spectral-domain interferometry (SDI) if modulators are to be used in its arms [14]. In addition, in a TB-based system such as those reported in [11, 12, 15, 16] a Mach-Zehnder configuration must be used in order to ensure a spatial separation between the footprints of the two beams on the diffraction grating or prism. In both cases, a splitter or a combination of splitters are employed to direct the output of the two arms of the interferometer towards the spectrometer.

We present here a configuration where such splitter is replaced by a pair of tilted diffraction gratings, illuminated by the two beams to be interfered at an angle. Such a configuration achieves two goals: (i) performs superposition of the two beams after their diffraction, in line with the TB procedure mentioned above and (ii) prevents the possibility to interfere for any part of the two beams that may fall on the same grating, securing no mirror terms even when some parts of the beams overlap. This means that a behavior as shown by the curve C_3 in Fig. 1 (visibility restricted to a single OPD sign) is always obtained, irrespective of the gap between the two beams.

As shown in Fig. 2 a Mach-Zehnder interferometer is implemented, employing two directional couplers: *S1* splits the optical power between the two arms, object and reference, and *S2*, which diverts and collects light from the object, *O*, via lens *L3*. In the reference arm, lenses *L1* and *L2* are used to route a collimating beam via two mirrors, *M1* and *M2* placed on a translation stage, *TS*, used to adjust the reference path length and thus vary the channeled spectrum modulation frequency, enabling the study of the visibility profile of the spectrometer for different OPD values. Lens *L2* focuses light into a single mode fiber, *SMFR*, whose end is placed in a groove with the fiber end from the object arm, brought from *S2* via *SMFO*. The two single-mode fibers (SMF) are closely laid together inside the groove, with their plastic buffers removed to minimize the distance between their tips. The two fiber ends are placed in the focal plane of lens *L4*. Each beam travels to a diffraction grating wherefrom the diffracted fan of rays is made convergent for each individual spectral component on a line camera *CMOS*, via a lens *L5*.

Due to the gap δ between the two SMF apertures, the two beams intersect at a distance f_4 from the lens *L4*, corresponding to the back focal plane of the lens *L4*. Because the directions of the two beams are divergent, if a single grating was used, rays of the same wavelength in the two beams would not superpose on the same pixel of the line camera. Therefore, a separate grating (*DG1,2*) is used for each beam. By tilting the two gratings in relation to each other, rays of the same wavelength are superposed on the line camera, implementing in this way the 2nd operation - interference - after the 1st operation, diffraction. Therefore, each of the two diffraction gratings is mounted on an individual rotation stage. By rotating these stages, the diffracted rays of similar wavelength are made parallel in their way towards the spectrometer lens, *L5*. Let us consider the angle θ between the two collimated beams emerging from *L4*, as depicted in the diagram in Fig. 2. Following a trigonometric analysis, such angle can be approximated by $\tan\theta \approx \delta/(2f_4)$, and given that $f_4 \gg \delta$ we have $\theta \ll 1$. The correction required for the angle between the two gratings is effectively less than 1 degree, therefore it cannot be visible in the sketch.

Further on from the back focal plane of *L4*, the beam directions will diverge and the distance between their centers will scale with the distance L_{grat} between *L4* and the pair of diffraction gratings *DG1-2*.

In order to employ the theory developed in previous reports [12, 17], an equivalent gap g is inferred from the present configuration and extrapolated to the case of a conventional Talbot Bands configuration using parallel beams incident on a single *DG*. It can be shown that at the grating level, the gap g between the two beams is approximately given by

$$g = \frac{1}{\cos\alpha}\frac{\delta}{2f_4}\left(L_{grat} - f_4\right), \quad \textbf{(1)}$$

where α is the angle between the axis of the lens *L4* and the normal $\hat{n}$ to the grating surface.

Moreover, the number of grating lines illuminated by each beam determines the width of the C profile versus OPD, as described in [11, 15]. This can be adjusted by varying the focal length f_4 of the lens *L4*, which changes the beam diameter S of the footprint on the grating.

From one grating groove to the next, the delay between the diffracted rays in the first order of diffraction amounts to λ_0 [2]. The equivalent number of grating grooves within the gap is given by $N = g/a$, where a is the grating groove periodicity. Therefore, according to the Talbot Bands theory [2], the profile of modulation contrast versus OPD, C, is shifted by $N\lambda_0$. The OPD value where C exhibits a maximum, OPD_{max}, is shifted from $OPD = 0$ by the same amount [12]:

$$OPD_{max} = \frac{g}{a}\lambda_0 \quad \textbf{(2)}$$

Given the wavelength used, $\lambda_0 = 831$ nm, and the grating groove periodicity of $a \sim 0.833$ μm, $\lambda_0/a = 0.831/0.833 \approx 1$, so $OPD_{max} \sim g$. Hence, by controlling the size of the gap g through manipulation of both L_{grat} and f_4 it is possible to achieve the same functionality as that previously reported [12, 15, 16], where a beam-splitter was used to direct the two spatially separated parallel beams onto the diffraction grating.

In order to characterize the visibility curves C of the system, several sets of measurements relating the channeled spectrum modulation to the OPD in the interferometer were carried out for different values of the gap g. These measurements were performed by recording the amplitude of the channeled spectrum modulation (obtained from the Fourier transform of the re-sampled spectrum) for several OPD values, which were varied in 20 μm increments using the *TS*. Different values of g were achieved by varying geometrical parameters of the spectrometer, namely the length L_{grat} between the collimating lens *L4* and the pair of diffraction gratings *DG1-2*, and also the focal length f_4 of the lens *L4*. Such changes allow g to be adjusted in the range of 1 to several mm, however an exact measure of it is difficult because the edges of the two diffraction gratings are contributing to the error in its determination. Estimation of the

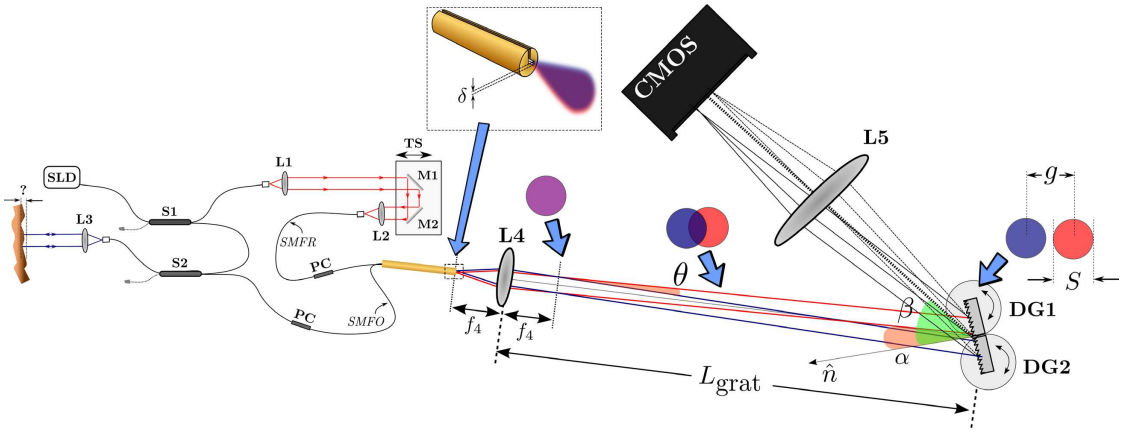

Fig. 2. *(color online)* Experimental set-up. **SLD**: superluminiscent diode (Superlum SLD-381-HP1-DIL-SM-PD, $\lambda_0 = 831.1$ nm, $\Delta\lambda = 16$ nm, ~ 10 mW output power); **S1-2**: fiber-based directional couplers; **L1-5**: achromatic lenses; **TS**: translation stage; **M1-2**: flat silver mirrors; **PC**: fiber-based polarization controllers; **DG1-2**: ruled diffraction gratings operating in reflection (Thorlabs GR25-1210, 1200 l/mm @ 1 μm); **CMOS**: line camera pixel array (Basler sprint spl-140km, 140 klines/s). Inset: the two output fibers (*SMFR* and *SMFO*) aligned inside the groove.

gap values are obtained by fitting curves obtained by theory to the experimental data, using numerical simulations based upon a code produced by Hughes [18]. This code, which was also used to produce the curves $C_1 - C_3$ in Fig. 1, performed a cross-correlation of the beam profiles from the two arms of the interferometer, whose result was multiplied by the *sinc* factor adjusted to the spectrometer's sampling resolution. In practice, the beam profiles are not top hats, as considered for simplicity in Fig. 1, but Gaussian, therefore the simulation used Gaussian profiles.

According to Eq. (1), the larger the length L_{grat}, the larger the gap g between the two spots (measured in an equivalent Talbot Bands spectrometer using a single grating). In turn, the larger the gap g, the larger the intrinsic delay between the two diffracted waves, leading to a shift of the C profile along the OPD axis, as mentioned earlier. On the other hand, modifying f_4 changes both OPD_{max} through g (given that $g \propto 1/f_4$) and the width of the C profile, given that the number of illuminated grating lines depends on the size of the footprint of the beam illuminating the grating, as described in [2, 11].

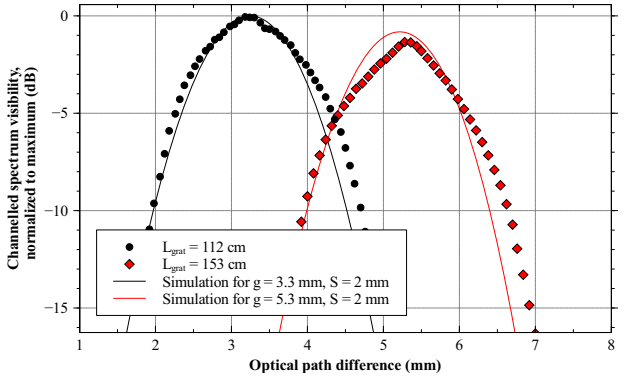

Fig. 3. *(color online)* Visibility profile versus OPD for the configuration in Fig.1 with $f_4 = 30$ mm, for two values of L_{grat} (112 cm, black circles and 153 cm, red diamonds, corresponding to a g value of $\sim$ 3.25 mm and $\sim$ 5.25 mm, respectively).

In the first set of measurements, only the gap g was modified by opting for two L_{grat} values separated by approximately 40 cm, accomplished by moving the group comprising the pair of diffraction gratings *DG1-2*, the *CMOS* camera, and the lens *L5* together along a direction given by the axis of *L4*. The results obtained are shown in Fig. 3. Considering the focal length of *L4*, $f_4 = 30$ mm and the projection angle $\alpha \sim 18$ degrees, the spot diameter of each beam on each grating is approximately $S \sim 2$ mm. Employing for simplicity, as in Fig. 1, a top hat power distribution within the footprint of each beam on the diffraction grating [2], the number of illuminated grating lines in each beam is $N = S/a = 2,400$. Cross-correlation of the two top hats, each of width $N\lambda_0$, leads to a triangular shaped C profile (as shown in Fig. 1) covering a $2N\lambda_0$ base of ~ 4 mm. As expected, when considering more real Gaussian footprints, the effective C width is smaller than $2N\lambda_0$, as shown by the -10 dB width (3 mm) of the simulated profiles in solid line overlaid on the experimental data in Fig. 3.

The second graph in Fig. 3 corresponds to a larger distance L_{grat} which determines a gap g larger than the beam diameter S. This experiment shows that due to a larger gap g the C profile moves to larger OPD values, as expected [12]. The shift on the visibility profile C towards larger OPD values presents the disadvantage of a decrease in visibility due to the spectrometer resolution (smaller values of the *sinc* factor as seen in Fig. 1).

The gap settings for the theoretical simulations were adjusted to fit the experimental curves, with a value of 3.3 mm for the $L_{grat} = 112$ cm case and a value of 5.3 mm for the $L_{grat} = 153$ cm case. Both experimental and theoretical data sets are normalized to the peak visibility of their respective data set. The $L_{grat} = 153$ cm experimental data set has a peak value ~ 1 dB lower than the corresponding simulation data, this may be due to an imperfect alignment of the spectrometer after being reassembled following the change in L_{grat}.

A second set of experiments refer to the effect of the focal length f_4 of lens *L4* on the visibility profile versus OPD. Fig. 4 illustrates the visibility decay with OPD for two f_4 values, using $L_{grat} = 153$ cm. The profile corresponding to $f_4 = 50$ mm displays a slight shift towards OPD = 0. Given that the gap is inversely proportional to f_4, a larger focal length yields a smaller gap g between the beams. However, increasing f_4 demands a proportionally larger L_{grat} value in order to achieve complete separation of the two beams. Furthermore, not achieving complete separation of the beams would lead to some parts of the two beams being diffracted by both gratings. These parts do not interfere, as commented above, reducing the overall interferometer performance.

The gap setting supplied to the simulations for $f_4 = 50$ mm

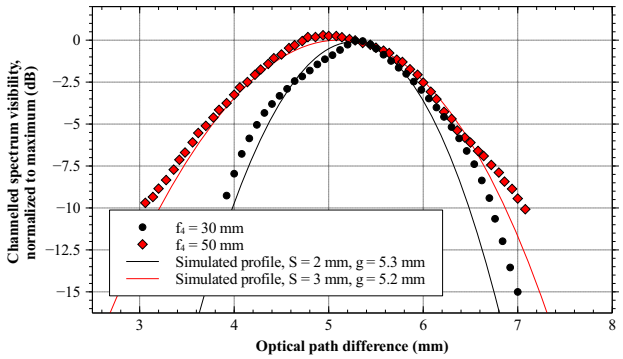

Fig. 4. *(color online)* Visibility profile versus OPD for the configuration with $L_{grat} = 153$ cm, for two values (black circles: $f_4 = 30$ mm, red diamonds: $f_4 = 50$ mm. Both experimental and theoretical data sets have been normalized to the peak value for the profile closer to OPD = 0.

is $g = 5.2$ mm. Due to implementation challenges it proved difficult to ensure that the beam centers remained in the same relative positions during the spatial adjustments of the components. In addition, the effective areas of the diffraction gratings do not extend up to their support edges and this contributes to the gap between the two beams. All these aspects make it difficult to accurately measure the gap g experimentally.

The beam diameter assumed $S = 3$ mm matches the experimental data, yielding a visibility profile width (FHWM) of around 2 mm. The peak location shifts towards smaller OPD values by ~ 0.4 mm, as shown in Fig. 4.

In conclusion, a novel Talbot Bands configuration is proposed, where the launching of the two beams from the object and reference arms uses a single lens and where the splitter before the spectrometer is eliminated by using two tilted diffraction gratings. The two tilted gratings perform two functions: (i) allow superposition of the two diffracted beams on the line camera and (ii) due to their tilt, overlapped parts of the beams incident on each grating do not contribute to interference, leading to total elimination of the mirror terms. The adjustment of the relative tilt of the gratings is not more difficult than the alignment demanded by the beam-splitter conventionally used in front of the spectrometer in previous reports [12, 15, 16].

Elimination of the final splitter also brings advantages in terms of power efficiency, as all the optical power arriving at the diffraction gratings from both beams can be directed towards the detector array. In a conventional system with a splitter up to 50% of the incident power is lost to the unused port of the splitter. Moreover, since both beams encounter optical elements with similar properties this set-up may present an extra advantage when handling large bandwidth signals as the splitting ratio of splitters depends on wavelength. Also, the eventual polarization disturbances introduced by the splitter are avoided.

From previous studies of Talbot band configurations [11, 12] it is known that a smaller gap is desired to shift the visibility curve closer to OPD=0 (Fig. 1, curve C_2). It is also known that if a larger axial range is desired, then C needs to be widened, which can be achieved by increasing f_4. However, this may lead to some overlap of the two beams before each grating, which associated with the fact that the two beams are diverging from each other means that the optical power diffracted in the overlapped region will not contribute to the interference. This is not due to the Talbot bands configuration (i.e., not due to the gap between the two incident beams), but simply to the fact that rays of similar wavelength in the two beams are not diffracted along parallel directions due to the initial angle between the beams before diffraction. This particularity of the system effectively impedes mirror terms from arising at all, hence it is not possible to observe a behavior similar to that of curves C_1 and C_2 in Fig. 1. In addition, the SNR is also reduced since the optical power available for interference is lower than that if the full beam footprint was illuminating a single grating.

A compromise has to be made in respect to the size of the gap between the two beams. It is known from previous reports on Talbot Bands that the shift of the visibility profile versus OPD towards larger OPD values, typical for Talbot band operation, leads to a lower visibility due to the factor C being moved to OPD values where the *sinc* factor is lower. Therefore, the gain in efficiency due to elimination of the final splitter somewhat compensates this reduction in visibility.

Additionally, in order to ensure complete separation between the two beams just before the gratings, L_{grat} needs to be large (over 1 m). Assuming complete beam separation, from Eq. (1) and using the identity $\tan\theta \sim \frac{\delta}{2f_4} \sim \frac{g}{L_{grat}}$ we can write L_{grat} as

$$L_{grat} = f_4 \left(1 + \frac{2}{\delta}\cos\alpha\right). \quad (3)$$

To reduce L_{grat} one can either reduce f_4 or increase δ. The former determines the size of the footprint on each grating, which then determines the number of grating lines illuminated and ultimately the width of the profile C and thus the axial range; the latter can be increased by separating the fibers in the launcher. There is a limit to this increase, since the larger the value of δ, the larger the aberrations via lens *L4* due to the beams originating from off-axis-placed cores.

Acknowledgements: This work was supported by the ERC under the EU's 7th Framework Programme, 'COGATIMABIO', No. 249889. A. Podoleanu is also supported by the NIHR Biomedical Research Centre at Moorfields Eye Hospital NHS Foundation Trust and UCL Inst. of Ophthalmology. M. Marques acknowledges the support of the Univ. of Kent in his PhD scholarship.

REFERENCES

1. H. F. Talbot, Philos. Mag **10**, 364 (1837).
2. A. G. Podoleanu, Opt. Express **15**, 9867–9876 (2007).
3. Z. Benko, M. Hilbert, and Z. Bor, Am. J. Phys. **68**, 513 (2000).
4. A. L. King, Am. J. Phys. **39**, 1195 (1971).
5. B. Baumann, M. Pircher, E. Götzinger, and C. K. Hitzenberger, Opt. Express **15**, 13375–13387 (2007).
6. E.Götzinger, M. Pircher, R. Leitgeb, and C. Hitzenberger, Opt. Express **13**(2), 583–594 (2005).
7. M.V. Sarunic, M. A. Choma, C. H.Yang, and J.A. Izatt, Opt. Express **13**(3), 957–967 (2005).
8. J. Zhang, J. S. Nelson, and Z. Chen, Opt. Lett. **30**, 147–149 (2005)
9. H. Bernd, B. Považay, A. Unterhuber, L. Wang, B. Hermann, S. Rey, G. Matz, and W. Drexler, Opt. Express **18**(5), 4898–4919 (2010).
10. M. Wojtkowski, R. Leitgeb, A. Kowalczyk, T. Bajraszewski, and A. F. Fercher, J. Biomed. Opt. **7**, 457–463 (2002).
11. D. Woods and A. G. Podoleanu, Opt. Express **16**, 9654–9670 (2008).
12. A. Bradu and A. G. Podoleanu, J. Biomed. Opt. **16**, 76010 (2011).
13. Z. Hu, Y. Pan, and A. M. Rollins, Appl. Opt. **46**, 8499 (2007).
14. M. E. Brezinski, *Optical Coherence Tomography: Principles and Applications* (Academic Press, 2006), p151.
15. P. Bouchal, A. Bradu, and A. G. Podoleanu, Opt. Express **20**, 5368–5383 (2012).
16. M. J. Marques, A. Bradu, and A. G. Podoleanu, Biomed. Opt. Express **5**, 1428 (2014).
17. M. Hughes, D. Woods, and A. G. Podoleanu, Electron. Lett. **45**, 182–183 (2009).
18. M. Hughes, Ph.D. thesis, University of Kent (2010). Online: http://www.mike-hughes.org/files/phd_oct_for_art.pdf